

APPENDIX

We wish to treat the case of a thin slab ($\Delta z \ll \lambda$) of excited harmonic oscillators. The surface density of oscillators is $\sigma = N\Delta z$. The displacement can be represented in terms of a slowly varying envelope:

$$X(t, z) = \exp(i\omega_0 t) \delta(z) \mathfrak{X}(t), \quad (\text{A1})$$

where $\delta(z)$ is the Dirac δ function. We require a solution that is symmetric in the forward and backward directions. One can verify that such a solution for Eqs. (4) and (A1) is

$$E(t, z) = -i\pi e f^{1/2} \omega_0^2 c^{-2} \{ \theta(z) \exp[i\omega_0(t - z/c)] + \theta(-z) \exp[i\omega_0(t + z/c)] \}, \quad (\text{A2})$$

where derivatives of $\mathfrak{X}(t)$ have been dropped and $\theta(z)$ is the step function. The harmonic oscillator equation (3) for $\gamma = 0$ becomes

$$\frac{d\mathfrak{X}(t)}{dt} = -\frac{1}{2}\Gamma \mathfrak{X}(t), \quad (\text{A3})$$

with $\Gamma = \pi f \omega_0 \sigma / mc^2$, where we have kept only first derivatives of $\mathfrak{X}(t)$. Equation (A3) leads to exponential decay of the stored energy W :

$$W(t) = W(0) e^{-\Gamma t}. \quad (\text{A4})$$

The decay rate Γ is proportional to the number of oscillators, as is characteristic of a coherent process.

Optical and Electron-Spin-Resonance Studies of Fourth-Nearest-Neighbor Chromium Ion Pairs in Ruby*†

M. J. BERGGREN

Department of Physics, Stanford University, Stanford, California 94305

AND

G. F. IMBUSCH‡

Bell Telephone Laboratories, Murray Hill, New Jersey 07974

AND

P. L. SCOTT

Natural Sciences Division, University of California, Santa Cruz, California 95060

(Received 19 June 1969)

The fine structure of the optical fluorescence spectrum arising from the fourth-nearest-neighbor chromium ion pair system in ruby is studied using high-resolution optical spectroscopy, ordinary electron-spin resonance, and optically detected electron-spin resonance. The ground-state energy levels of this system are found to be describable by a simple spin Hamiltonian of the form

$$\mathcal{H} = g\beta \mathbf{H} \cdot \mathbf{S} + J/2[S(S+1) - 15/2] + D_S[S_z^2 - \frac{1}{3}S(S+1)] + E_S[S_x^2 - S_y^2],$$

where the directions of the symmetry axes, D_S , and E_S each depend on the spin S in a predictable way, requiring only two adjustable parameters: D_C (the usual second-order crystal-field term of axial symmetry) and D_E (a similar term arising from the anisotropic exchange interaction). The value of D_C is found to be $-0.191 \pm 0.005 \text{ cm}^{-1}$, which is equal to that for the isolated ion. The value of D_E is found to be $-0.021 \pm 0.005 \text{ cm}^{-1}$. A phonon-assisted energy-transfer mechanism is postulated to account for the existence of the optically detected spin-resonance spectrum.

I. INTRODUCTION

A SUBSTANTIAL amount of attention has been given to the subject of chromium ion pairs in ruby ($\alpha\text{-Al}_2\text{O}_3:\text{Cr}^{3+}$) over the past several years. In particular, experimental work on the optical spectrum,¹

* Work supported in part by the Advanced Research Projects Agency, under Contract No. SD 87 G-704, and in part by the Office of Naval Research, under Grant No. N00014-68-A-0381-0002.

† Based on part of the Ph.D. dissertation of M. J. Berggren, Stanford University, 1969 (unpublished).

‡ Present address: University College, Galway, Ireland.

¹ L. F. Mollenauer and A. L. Schawlow, *Phys. Rev.* **168**, 309 (1968); and references therein.

and on the paramagnetic resonance spectrum,²⁻⁵ as well as theoretical work on systems of such pairs of

² L. Rimai, H. Statz, M. J. Weber, G. A. de Mars, and G. F. Koster, *Phys. Rev. Letters* **4**, 125 (1960); *J. Appl. Phys.* **32**, 2185 (1961); *J. Phys. Soc. Japan* **17**, Suppl. B-1, 430 (1962).

³ Yu. L. Shelekin, M. P. Votinov, and B. P. Berkovskii, *Fiz. Tverd. Tela.* **8**, 589 (1966); **9**, 2119 (1967) [English transl.: *Soviet Phys.—Solid State* **8**, 469 (1966); **9**, 1663 (1967)].

⁴ W. Gunsser, W. Hille, and A. Knappwost, *Z. Phys. Chem.* **58**, 316 (1968).

⁵ A. Jelenski, H. Szymczak, and J. Twarowski. *Proceedings of the International Conference on Magnetic Resonance and Relaxation, Fourteenth Colloque Ampere, Ljubljona, Yugoslavia, 1966*, edited by R. Blinc (North-Holland Publishing Co., Amsterdam, 1967), p. 1205.

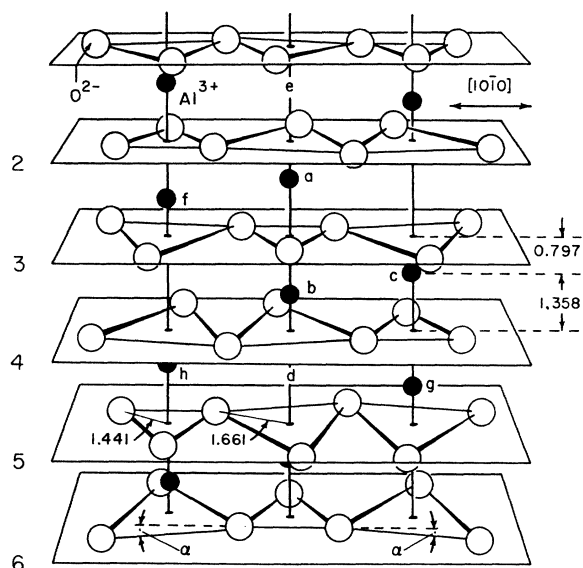


FIG. 1. Portion of the Al_2O_3 lattice (from Geschwind and Remeika), showing the geometrical relationships of the various pair types. The black circles represent aluminum ions (for which chromium ions may be substituted) the white circles represent oxygen ions. If ion b is a reference ion, a is a first-nearest neighbor, c is a second-nearest neighbor, h is a third-nearest neighbor, and f and g are fourth-nearest neighbors. The C_3 axis is vertical, and all of the aluminum ions shown lie in one of the three equivalent mirror planes.

ions⁶⁻⁸ have contributed substantially to the understanding of the nature of the coupling of the first four near-neighbor pair types.

In general, the ground states of such pairs seem to be reasonably well described by a Hamiltonian of the form

$$\mathcal{H} = \mathcal{H}_a + \mathcal{H}_b + \mathcal{H}_{\text{ex}}, \quad (1)$$

where \mathcal{H}_a and \mathcal{H}_b are the single-ion Hamiltonians of ions a and b in the absence of any interaction, and

$$\mathcal{H}_{\text{ex}} = J \mathbf{S}_a \cdot \mathbf{S}_b + j (\mathbf{S}_a \cdot \mathbf{S}_b)^2 + V_{ab}. \quad (2)$$

Here S_a and S_b are the spins of the ions a and b . V_{ab} is a term which describes any remaining interaction between the ions which is not attributable to the terms in J or j , and is usually small, giving rise to splittings

TABLE I. Exchange parameters for the first four near-neighbor pair types. Units are cm^{-1} .

Near-neighbor pair type	J	j
first	240	?
second	83.6	-9.7
third	11.59	0.06
fourth	-6.99	0.14

⁶ A. M. Clogston, Bell Telephone Laboratories International Report, 1959 (unpublished).

⁷ J. Ferguson, H. J. Guggenheim, and Y. Tanabe, *J. Chem. Phys.* **45**, 1134 (1966).

⁸ M. H. L. Pryce (to be published).

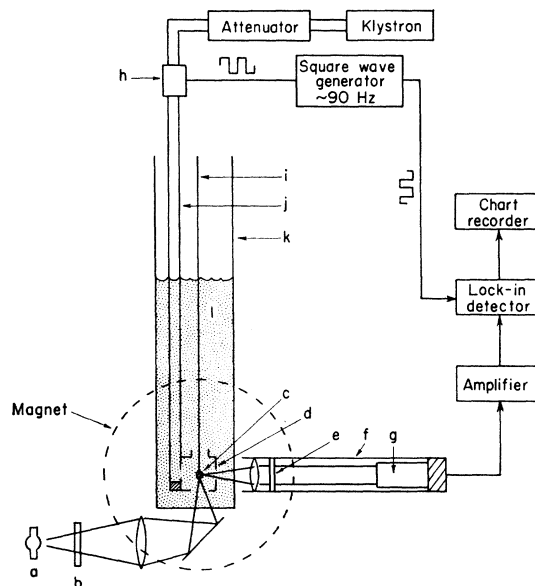


FIG. 2. Schematic diagram of apparatus for optical detection of spin resonances. a, 200-W mercury short-arc lamp; b, copper-sulfate filter; c, ruby sample; d, microwave cavity; e, 7009 Å narrow-band interference filter; f, light pipe; g, S-20 phototube; h, microwave modulator; i, shaft for rotating sample; j, waveguide; k, helium Dewar; l, liquid helium.

of less than 1 cm^{-1} . Some of the principle findings reported and analyzed in this paper relate to the nature of V_{ab} .

The present state of our knowledge regarding the first four near-neighbor pair types (for the geometrical relationships of these pairs, see Fig. 1) is summarized in Table I, where we tabulate values of J and j obtained by a least-squares fit of observed ground-state energy levels⁹ to a Hamiltonian of the form of Eq. (2), in which V_{ab} has been neglected.

The optically excited states of such pairs appear to require a more general form of \mathcal{H}_{ex} for their description,⁸⁻¹⁰ given by

$$\mathcal{H}_{\text{ex}} = \sum_{ij} J_{ij} (\mathbf{s}_{ai} \cdot \mathbf{s}_{bj}), \quad (3)$$

where s_{ai} and s_{bj} are the spins of electrons occupying the various one-electron orbitals on ions a and b . In this expression, the smaller biquadratic terms have been neglected.

In the following sections, we shall concern ourselves mainly with the fourth-nearest-neighbor pair types, and with the detailed splittings of energy levels, especially in the ground states. In particular, this will involve an investigation of the detailed nature of the term V_{ab} in Eq. (2).

⁹ P. Kisluk, N. C. Chang, P. L. Scott, and M. H. L. Pryce, *Phys. Rev.* **184**, 367 (1969).

¹⁰ R. J. Birgeneau, *J. Chem. Phys.* **50**, 4282 (1969).

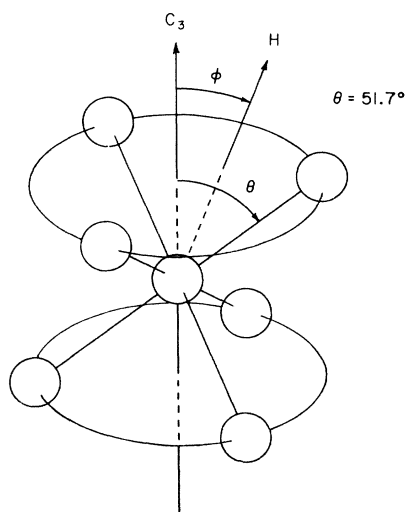


FIG. 3. Geometrical relationships of fourth-nearest neighbors, showing a central reference ion with the six symmetrically placed fourth-nearest-neighbor sites. Oxygen ions are not shown. The C_3 axis, the external magnetic field, and one of the fourth-nearest-neighbor axes all lie in a mirror plane.

II. EXPERIMENTAL TECHNIQUES

Three different kinds of experiments were used to investigate the behavior of the energy levels of the fourth-nearest-neighbor ion pairs: (1) high-resolution optical fluorescence, (2) ordinary electron spin resonance (ESR), and (3) optically detected spin resonance. These techniques are described in this section.

A. High-Resolution Optical Fluorescence

In these experiments, a 1.8-m Jarrell-Ash scanning spectrometer was used to observe the optical fluorescence in a high-quality Linde ruby rod of 0.05% chromium ion concentration. Even at this relatively low concentration, many of the pair lines are quite strong in fluorescence, and the strain broadening is less than in more concentrated rubies. Nevertheless, in all cases the resolution was limited by the strain broadening of the lines. Generally, the splittings of the various components of the lines could be measured to within an uncertainty of $\pm 0.02 \text{ cm}^{-1}$. In all cases, the fluorescence was excited using a high-pressure mercury arc lamp filtered by $\sim 1 \text{ cm}$ of saturated copper sulfate solution. The Zeeman effect of some of the pair lines was observed, using magnetic fields between 0 and 16 kG.

B. Ordinary ESR

In these experiments, ESR was observed using an ordinary crystal-video microwave spectrometer operating at frequencies between 24 and 37 GHz, with magnetic fields between 0 and 19 kG. High sensitivity was obtained by using high-frequency field modulation ($\sim 40 \text{ kHz}$) introduced via a stiff wire loop inside a TE_{012} -mode cavity. Ruby samples of approximately

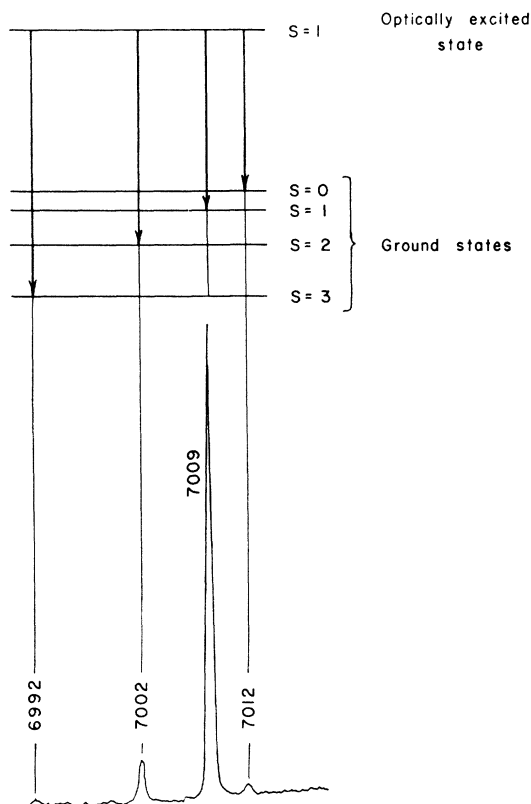


FIG. 4. Group of fluorescence lines arising from the fourth-nearest-neighbor pair system at $T=2^\circ\text{K}$. The relevant energy levels are also shown.

0.3% chromium ion concentration were used. In a few instances, a superheterodyne detection scheme was used to avoid saturation of the resonances at low temperatures.

C. Optically Detected ESR

In these experiments, the ESR's associated mainly with the fourth-nearest-neighbor pair types were

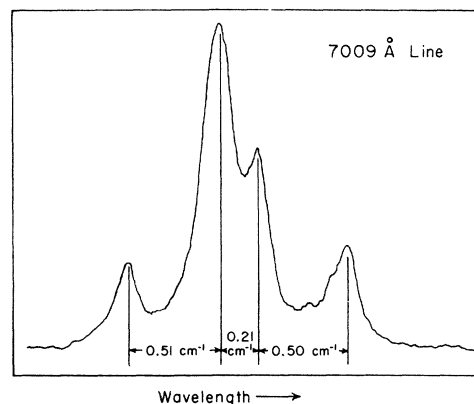


FIG. 5. 7009 Å line seen under high resolution.

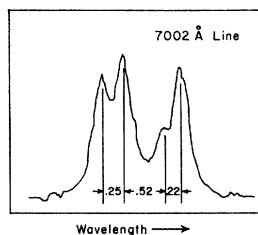


FIG. 7. 7002 Å line seen under high resolution. Splittings shown are in cm^{-1} .

observed by monitoring the fluorescent intensity of the N_2 line at 7009 Å, while simultaneously irradiating the crystal with microwave radiation. Figure 2 shows a block diagram of the experimental arrangement. In this apparatus, the ruby sample, which is supported inside the microwave cavity and immersed in liquid helium, is pumped with a filtered 200-W mercury arc lamp in the usual way. The fluorescent intensity in the vicinity of 7009 Å is monitored using a narrow-band interference filter of 5-Å bandwidth¹¹ and a photomultiplier tube with an $S-20$ response. The microwave radiation is chopped at ~ 90 Hz using a microwave modulator, and the 90-Hz component of the 7009 Å fluorescence is monitored using a P.A.R. lock-in detector as the magnetic field is swept. Since the N_2 -line fluorescence at 7009 Å has been shown to arise from fourth-nearest-neighbor pair types,¹ we might expect that resonances seen by use of this technique would arise mainly from microwave transitions within the fourth-nearest-neighbor system. As we shall discuss in the following paragraphs, this in fact appears to be the case.

Before discussing the detailed nature of the various spectra, we review the geometrical relationships of the various near-neighbor pair types. Figure 1 shows a portion of the Al_2O_3 lattice (taken from Geschwind and Remeika¹²). For any given reference ion, there is one possible first-nearest-neighbor site, three possible second-nearest-neighbor sites, three possible third-nearest-neighbor sites, and six possible fourth-nearest-neighbor sites. In Fig. 1, the crystal-line C_3 axis is vertical, and all of the aluminum ions shown in the figure lie in one of the three equivalent mirror planes. Perpendicular to the three mirror planes are three C_2 axes.

Since most of our discussion relates to fourth-nearest-neighbor pair types, we show in Fig. 3, the six equivalent sites which may be occupied by fourth-nearest

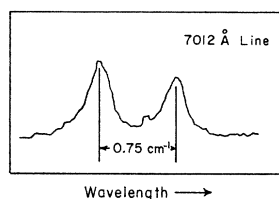


FIG. 6. 7012 Å line seen under high resolution.

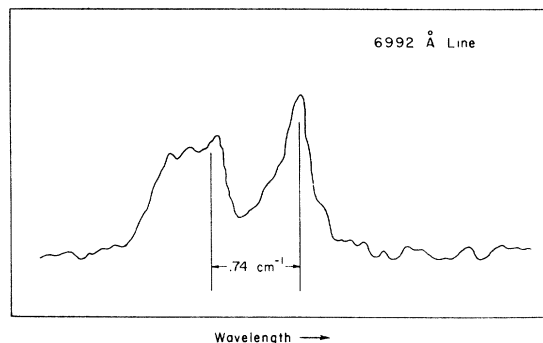


FIG. 8. 6992 Å line seen under high resolution. The 0.74- cm^{-1} splitting of the optically excited state is indicated.

neighbors. Note that any fourth-nearest-neighbor pair axis makes an angle $\theta = 51.7^\circ$ with the C_3 axis.

III. OPTICAL FLUORESCENCE SPECTRUM FROM FOURTH-NEAREST-NEIGHBOR PAIRS

The fluorescence spectrum at 4.2°K from the fourth-nearest-neighbor pair types and the set of energy levels associated with this spectrum are shown in Fig. 4. The line at 7009 Å is one of the strongest fluorescence lines in dark ruby, and is usually called the N_2 line. All four lines apparently originate from the lowest of the optically excited states of the fourth-nearest-neighbor pair system. It is labeled an $S=1$ state because it appears to behave as a spin triplet.¹³

Close examination of the four lines shown in Fig. 4 shows evidence of fine structure associated with each line. Figure 5 shows¹⁴ the structure for the N_2 -line fluorescence at 4.2°K. This structure may be presumed to arise from small splittings in the ground and excited states. In an attempt to deduce the origin of these splittings, we focus our attention first on the 7012 Å line, which presumably terminates on the $S=0$ state.

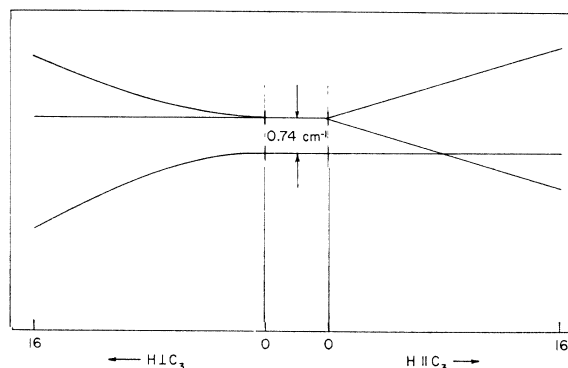


FIG. 9. Energy-level diagram of the lowest excited state of the fourth-nearest-neighbor system, as deduced from Zeeman studies of the 7012 Å line.

¹³ G. F. Imbusch and M. B. Graifman, *J. Appl. Phys.* **39**, 981 (1968).

¹⁴ A similar figure appears in A. L. Schawlow, *J. Appl. Phys.* **33**, 395 (1962).

¹¹ Obtained from Baird-Atomic Inc., Cambridge, Mass.

¹² S. Geschwind and J. P. Remeika, *Phys. Rev.* **122**, 757 (1961).

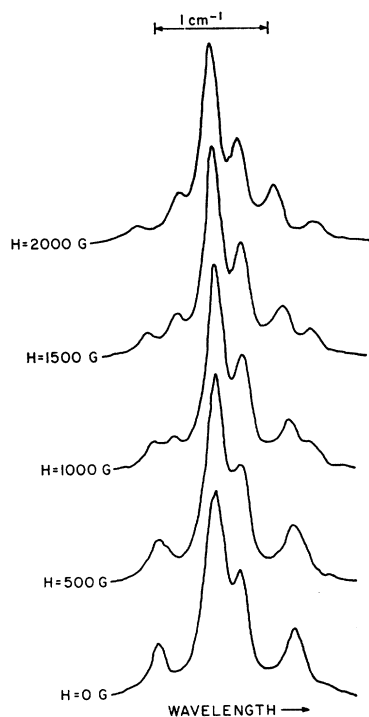


FIG. 10. Zeeman effect of the 7009 Å line, showing the splitting of the two outermost components.

Figure 6 shows this line as it appears at 4.2°K. Upon lowering the temperature to 1.4°K, the shorter wavelength component becomes weaker, indicating that the 0.74-cm⁻¹ splitting is associated with the excited state.

Next we look at the 7009 Å line, whose structure can be explained by assuming an excited-state splitting of 0.74 cm⁻¹, and a ground-state splitting of 0.51 cm⁻¹. Similarly, the structure of the 7002 Å line, whose fluorescence at 4.2°K is shown in Fig. 7, can be ex-

plained by assuming a 0.74-cm⁻¹ splitting in the excited state, and a 0.25-cm⁻¹ splitting in the ground state. The structure associated with the 6992 Å line, shown in Fig. 8, while not completely resolved, clearly shows the 0.74-cm⁻¹ excited-state splitting.

IV. ZEEMAN EFFECTS IN THE OPTICAL FLUORESCENCE SPECTRUM

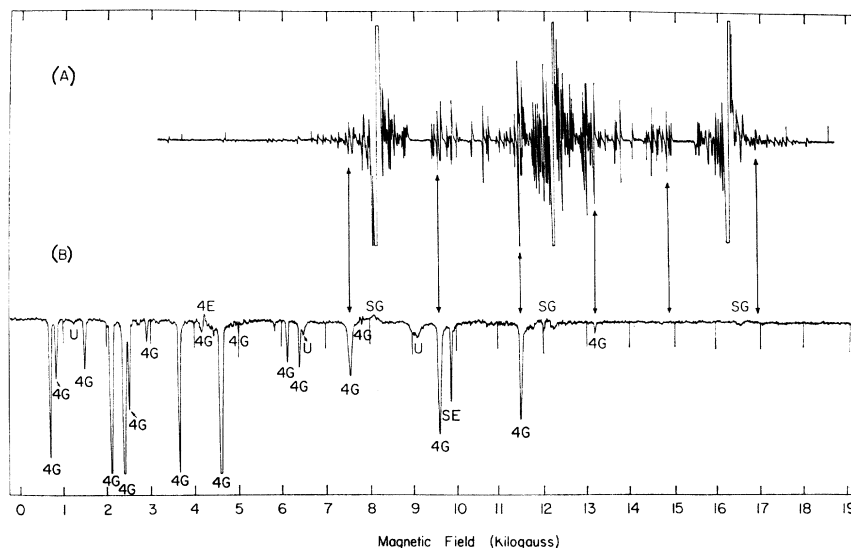
The splitting of the 7012 Å line (which ends on $S=0$) under an applied magnetic field leads us to make an energy-level diagram for the lowest excited state such as that shown in Fig. 9. We note that this excited state apparently behaves as a spin triplet ($S=1$), and that the axis of symmetry for this state appears to lie close to the C_3 axis of the crystal. Similar behavior has recently been observed by Kanskaya and Przhhevskii for this transition.¹⁵ Having determined the behavior of the excited state helps us to unravel the Zeeman splitting of the other ground-state levels by studying the optical Zeeman effect of the other fluorescence lines.

The 7009 Å line splits into six fairly well-defined components when a magnetic field of about 2 kG is applied along the C_3 axis, with each of the two outermost components splitting into two, while the two innermost components remain more or less unaffected, as shown in Fig. 10. This behavior leads us to describe the terminal state of the 7009 Å fluorescence as an $S=1$ state whose energy levels may be approximately described by a spin Hamiltonian of the form

$$\mathcal{H} = g\beta\mathbf{H} \cdot \mathbf{S} + D[S_z^2 - \frac{1}{3}S(S+1)] \quad (4)$$

with $g \cong 2.0$, and $D \cong 0.51$ cm⁻¹. It also appears that the axis of symmetry for this state lies fairly close to the C_3 axis. ESR data for this state are in agreement with these observations, as we shall see in Sec. V.

FIG. 11. Trace (A) (above): ordinary ESR spectrum, showing the derivative of the absorption versus H , of a 0.3% ruby, at room temperature, with H parallel to C_3 . The three strongest lines arise from isolated chromium ions; the remaining multitude of lines are probably due to exchange coupled pairs of various types and orientations. Trace (B) (below): optically detected ESR spectrum of the same sample at 2°K, with H parallel to C_3 . Increasing 7009 Å fluorescent intensity is downwards. All lines labeled 4G arise from the $S=3$ ground state of the fourth-nearest neighbors. The origin of other lines is described in the text. Both spectra were taken at a microwave frequency of ~ 35 GHz. The six arrows indicate corresponding fourth-nearest-neighbor resonances in the two spectra.



¹⁵ L. M. Kanskaya and A. K. Przhhevskii, *Opt. i Spektroskopiya* **26**, 226 (1969) [English transl.: *Opt. Spectry. (USSR)* **26**, 121 (1969)].

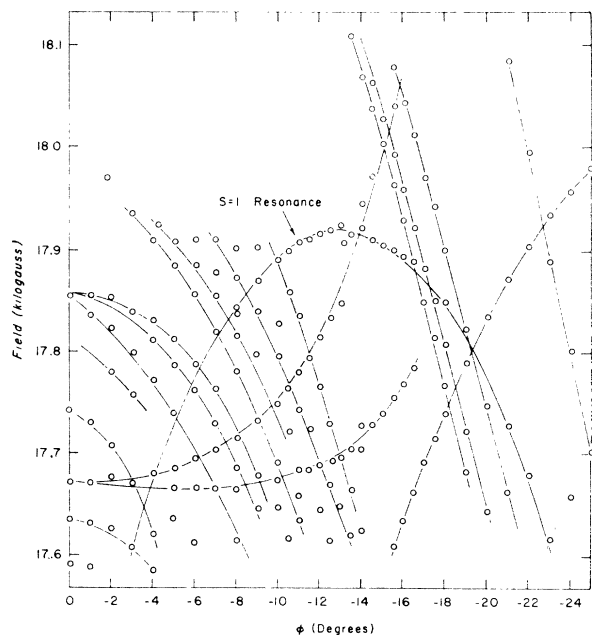


FIG. 12. Portion of a plot showing the positions of ordinary spin resonances as a function of the angle ϕ between the magnetic field and the C_3 axis. A resonance arising from the $S=1$ ground state of the fourth-nearest neighbors is shown.

The Zeeman effects of the 7002 and 6992 Å lines were not studied, but one would expect for both lines fairly complex, unresolved Zeeman patterns. As we shall see later, the axis of the $S=2$ terminal state of the 7002 Å line probably lies along the fourth-nearest-neighbor pair axis. Also both lines are fairly weak even in the absence of a magnetic field, and would be extremely difficult to study. Nevertheless, the fluorescence pattern of the 7002 Å line (Fig. 7) is consistent with the designation of the terminal state as an $S=2$ state whose levels are described by a spin Hamiltonian of the form of Eq. (4), with $D \cong -0.07 \text{ cm}^{-1}$. (The $M=0$ state would be split from the $M=\pm 1$ states by only 0.07 cm^{-1} , and would probably not be resolved, whereas the $M=\pm 2$ states would be split from the $M=\pm 1$ states by 0.21 cm^{-1} thus giving rise to the observed splitting of 0.25 cm^{-1} .)

V. ESR OF PAIR GROUND STATES

The room-temperature ESR spectrum of dark ruby consists of hundreds of lines, most of which are unresolved. A typical spectrum, taken at 35 GHz, with H parallel to the C_3 axis, is shown in Fig. 11(A). In general, there are six transitions arising from the $S=\frac{3}{2}$ ground state of the *single* Cr^{3+} ion, three of which are allowed, and three of which are more or less forbidden, depending upon the angle between the magnetic field and the C_3 axis. Most of the remaining lines probably arise from coupled pairs of chromium ions. We have focussed our attention on those ESR lines which are

well resolved, at least for some orientations of the magnetic field. The expectation is that at least some of these lines arise from the more strongly coupled ion pair systems, that is, the first- through fourth-nearest neighbors. This expectation turns out to be fulfilled.

A general examination of the resonance spectrum at room temperature was made by sweeping the magnetic field through the spectrum at each of many angles ϕ , where ϕ is the angle between the magnetic field H and the C_3 axis. H lies in a mirror plane, as shown in Fig. 3. By this technique, a large plot was constructed showing the positions of the resonances as a function of the angle ϕ . A small portion of such a plot is shown in Fig. 12, in which one of the resonances arises from the $S=1$ state of the ground states of the fourth-nearest-neighbor system. This resonance was searched for and found on the basis of the Zeeman studies of the 7009 Å line, and on the basis of predictions made by the theory developed in Sec. VII. The resonance may be described by a Hamiltonian such as given by Eq. (4), with $D=0.492 \text{ cm}^{-1}$, and with an axis of symmetry in the direction $\phi = -13^\circ$.

Of course, such plots will include many resonances which are irrelevant to our investigation of the fourth-nearest-neighbor pair system, since it will include resonances from all coupled pairs of various orientations in the crystal. Also, each coupled-pair ground state will have 16 energy levels in general, with possible resonances occurring between many of these 16 levels. Nevertheless, by using some of the techniques described below, considerable information may be obtained.

One of the simplest techniques involves lowering the temperature in order to depopulate energy levels. Of the first four nearest-neighbor pair types, the first, second, and third are all antiferromagnetically coupled, with the nonmagnetic $S=0$ singlet lying lowest. Only the fourth-nearest neighbor is ferromagnetically coupled, and at liquid-helium temperatures only the $S=3$ state of this system will be thermally populated. Hence, at liquid-helium temperatures, one expects to see only resonances from this state, in addition to single-ion resonances, and perhaps resonances from more weakly coupled systems. In addition, lowering the temperature from 4.2 to 1.5°K will change the relative intensities of the various resonances within the $S=3$ state in a more or less predictable way as the thermal populations change among the various M_s levels.

Another technique involves observing changes in the positions of the resonance lines when the microwave frequency is changed. By this technique, the relative slopes of energy levels with field can be observed, and in many instances allowed transitions ($\Delta M=1$) can be distinguished from forbidden transitions ($\Delta M=2, 3$, etc.). Using these techniques, several resonances were tentatively assigned to the $S=1$ and 3 states of the fourth-nearest neighbors, to be later confirmed using the techniques described in Sec. VI. Resonances from

the $S=2$ states were not observed. They are predicted by our theoretical analysis (Sec. VII) to lie in regions such that they are unresolvable from other lines in the spectrum.

VI. OPTICAL DETECTION OF FOURTH-NEAREST-NEIGHBOR PAIR RESONANCES

When the intensity of the 7009 Å fluorescence is monitored while simultaneously irradiating the crystal with microwaves and sweeping the magnetic field, a spectrum is observed, as shown in Fig. 11(B). As with the ordinary ESR spectrum, the positions of the resonance lines may be observed and plotted as a function of the angle φ . In addition, one may investigate the dependence of the line positions on the microwave frequency. One may also determine the dependence of the line *intensities* on microwave power, with the notion that the intensities of strongly allowed transitions may be less power-dependent than the more forbidden transitions. Using all three of these techniques, one can identify six resonances which correspond to the six $\Delta M = \pm 1$ allowed transitions within the $S=3$ multiplet of the fourth-nearest-neighbor ground state. These are indicated by the double-ended arrows in Fig. 11, which also indicate the corresponding resonances in the ordinary ESR spectrum. Those resonances not observed above ~ 14 kG in the optically detected spectrum are presumably absent because the energy levels involved in these resonances are not populated at 2.0°K, the temperature at which the spectrum was taken.

In analyzing this spectrum, we first attempt to fit the observed $\Delta M = \pm 1$ transitions using a simple spin Hamiltonian of the form

$$V_3 = g\beta\mathbf{H} \cdot \mathbf{S} + D_3[S^2 - \frac{1}{3}S(S+1)] + E_3[S_x^2 - S_y^2], \quad (5)$$

where the subscript 3 implies reference to the $S=3$ state. We find $D_3 = -0.096$ cm⁻¹, and $E_3 = -0.01$ cm⁻¹. We have taken $g=1.985$, the single-ion g value. In addition, we determine an axis of symmetry for this $S=3$ state at $\varphi=22.0^\circ$ (see Fig. 3). We then use a simple computer program to diagonalize V_3 for off-axis directions, and to plot the energy levels versus magnetic field H . Such a plot is shown in Fig. 13, for H parallel to C_3 . Note that when H is parallel to C_3 , it makes an angle of 51.7° with all fourth-nearest-neighbor pair axes, and presumably an angle of 22.0° with these $S=3$ -state symmetry axes. This plot of energy levels versus H may then be used to predict the positions of additional resonances, as shown by the arrows of Fig. 13. In this manner, one may predict, with an accuracy of ~ 50 G, all of the resonances labeled 4G (for fourth-nearest-neighbor ground state) shown in Fig. 11(B). We note that such an analysis accounts for the majority of the resonances appearing in the optically detected spectrum, and supports the notion that detecting pair resonances in this way serves to isolate those microwave transitions arising from a particular pair type.

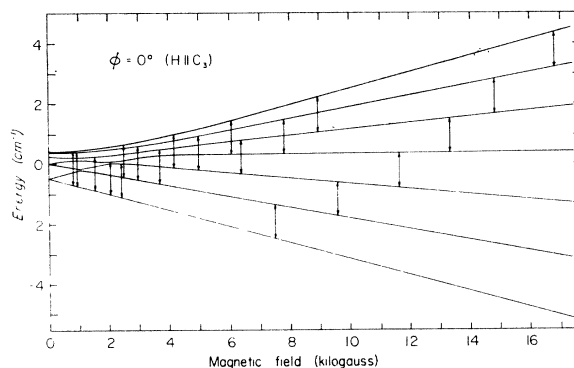


FIG. 13. Computer-generated plot of the energy levels versus magnetic field for the $S=3$ ground state of the fourth-nearest-neighbor pair system, using the spin Hamiltonian of Eq. (9), and the values of D_3 and E_3 given in Table II. All possible microwave transitions are indicated, and all but the two highest field transitions are observed as shown in Fig. 11(B).

A few additional resonances occurring in the spectrum shown in Fig. 11(B) are also of interest. The resonance marked 4E arises from the lowest of the optically excited states of the fourth-nearest neighbors, and provides evidence for the $S=1$ character of this state, as noted by Imbusch and Graifman.¹³ (A second resonance from this state would appear at $H=19.2$ kG, just beyond the range of our magnetic field for this particular run.) The sharp resonance marked SE in Fig. 11(B) arises from the optically excited 2E state of the single ion. The presence of this resonance, in addition to the broad resonances arising from the single-ion ground states, marked SG in Fig. 11(B), are an indication of the role played by the isolated chromium ions in the observation of these resonances, as discussed in the following paragraph. A few remaining weak resonances, marked U in Fig. 11(B), remain unassigned.

Of considerable interest is the mechanism by which these optically detected resonances are observed. Since the $S=3$ ground state of the fourth-nearest-neighbor pair system is neither the initial state nor the terminal state for the 7009 Å fluorescence, it is perhaps a little surprising that the resonances are seen at all. One rather curious feature of these resonances is that nearly all of them are seen as an *increase* in the 7009 Å fluorescent intensity. While we do not thoroughly understand the mechanism, it seems possible that it relies on energy transfer between the single ions and the fourth-nearest-neighbor pairs. A possible nonradiative-energy-transfer mechanism is shown in Fig. 14. Our supposition is that the efficiency of the energy transfer is enhanced when a fourth-nearest-neighbor-pair system is raised from a lower level of the $S=3$ multiplet to a higher level of this same multiplet through application of the appropriate microwave frequency. That is, in Fig. 14, the energy-transfer process labeled A is less efficient than that labeled B. The process shown A is a phonon-assisted process, with a phonon energy of about 120 cm⁻¹. Process A involves a slightly lower energy phonon than

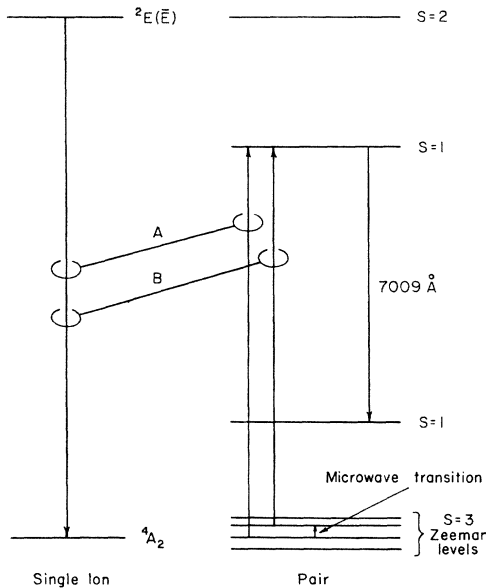


FIG. 14. A possible (phonon assisted) energy transfer mechanism giving rise to the observed optically detected ESR spectrum. Process *A* is presumed less efficient than process *B*, so that the total 7009 Å intensity increases when the microwave transition is induced. Only a selected few energy levels are shown, and are not to scale. Some additional energy transfer, not requiring phonons, may occur via the *S*=2 excited state of the pair, but does not appear to be primarily responsible for the observed spectrum.

process *B*, and since in this region the density of phonon states increases with increasing energy, we might expect process *A* to be less efficient, thus leading to an increase in 7009 Å intensity when a microwave transition is induced, as observed. Another possibility is that a resonant transfer of energy takes place, involving the *S*=2 excited state of the pair shown in Fig. 14, which is nearly coincident with the ${}^2E(\bar{E})$ excited state of the single ion.⁹ With this process, however, one might expect at least some of the *S*=3 microwave resonances to be observed as decreases in the 7009 Å intensity. While it is possible to conceive of other mechanisms involving only the energy levels of the pair, the fact that the single-ion resonances in both the 4A_2 ground state and the 2E excited states are observed in this spectrum lends support to the hypothesis of an energy transfer mechanism between the single ions and the pairs. It is also known from previous experiments that the abnormally strong fluorescence of the *N* lines owes its existence to such energy transfer.^{10,16}

VII. THEORY OF FOURTH-NEAREST-NEIGHBOR GROUND STATES

In light of the wealth of experimental data relating to the ground-state energy levels of the fourth-nearest-neighbor pair system (*S*=0, 1, 2, 3), it seems reasonable

¹⁶ G. F. Imbusch, Phys. Rev. **153**, 326 (1967).

to ask whether these levels can be described in terms of a simple spin Hamiltonian. We have already seen that the seven levels of the *S*=3 state can be described by the Hamiltonian V_3 [Eq. (5)]. We now attempt to generalize this to describe the remaining energy levels. As a starting point, we use a spin Hamiltonian which is a slight generalization of that used by Owen¹⁷:

$$V_S = g\beta\mathbf{H} \cdot \mathbf{S} + 3\alpha_S D_e [S_{z''}{}^2 - \frac{1}{3}S(S+1)] + \beta_S D_e [S_{z'}{}^2 - \frac{1}{3}S(S+1)]. \quad (6)$$

In this expression, *z''* is the direction of the pair axis, and *z'* is the direction of the *C*₃ axis. *S* is the total spin of the pair. *D_e* includes the axially symmetric anisotropic exchange interaction as well as the dipolar interaction:

$$D_e = D_E(\text{exchange}) + D_d(\text{dipole-dipole}),$$

where

$$D_d = -(g^2\beta^2/r_{ab}{}^3), \quad (7)$$

and *r_{ab}* is the separation between the two ions, about 3.57 Å for the fourth-nearest neighbors. *D_e* is the usual second-order crystal-field term with axial symmetry. Terms of rhombic symmetry, *E_e* and *E_c*, are neglected in our approximate theory. α_S and β_S are the operator equivalent factors given by Owen¹⁷:

$$\alpha_S = -\frac{1}{2} \left\{ \frac{S(S+1) + 4S_a(S_a+1)}{(2S-1)(2S+3)} \right\}, \quad (8a)$$

$$\beta_S = \frac{3S(S+1) - 3 - 4S_a(S_a+1)}{(2S-1)(2S+3)}, \quad (8b)$$

where *S_a* (= 3/2) is the spin of a single isolated ion.

In order to cast Eq. (6) into a form which can be compared with experiment, we write it with respect to a *single* set of symmetry axes (*x, y, z*):

$$V_S = g\beta\mathbf{H} \cdot \mathbf{S} + D_S [S_z^2 - \frac{1}{3}S(S+1)] + E_S [S_x^2 - S_y^2]. \quad (9)$$

The directions of these symmetry axes will depend on *S*, as will *D_S* and *E_S*. We choose the *x-z* plane to be that

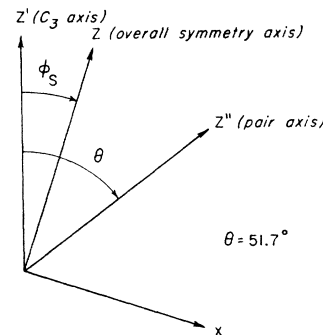


FIG. 15. Diagram showing the relationships of the various axes of symmetry. All axes, including the *x* axis, lie in the plane of the paper, which is a mirror plane.

¹⁷ J. Owen, J. Appl. Phys. **32**, 213S (1961).

TABLE II. Parameters of fourth-nearest-neighbor ground-state energy levels.

Spin	Parameter	Value from optical data ^a	Value from ESR data ^a	Theoretical value
S = 1	φ_1	small	$-13^\circ \pm 1^\circ$	-14.3°
	D_1	$0.51 \pm 0.02 \text{ cm}^{-1}$	0.492 cm^{-1}	0.491 cm^{-1}
	E_1	unresolved ^b		-0.10 cm^{-1}
S = 2	φ_2			-51.7°
	D_2	$-0.075 \pm 0.02 \text{ cm}^{-1}$		-0.087 cm^{-1}
	E_2	unresolved ^b		0
S = 3	φ_3		$+22^\circ \pm 1^\circ$	$+19.2^\circ$
	D_3	unresolved ^b	-0.0965 cm^{-1}	-0.0935 cm^{-1}
	E_3	unresolved ^b	-0.01 cm^{-1}	-0.011 cm^{-1}

^a A blank in the Table implies that the parameter was not determinable by this method.

^b In these cases, the theoretically predicted splittings are smaller than the observed strain-broadened linewidth.

containing both the C_3 axis and the pair axis (i.e., a mirror plane) as shown in Fig. 15. φ_S designates the direction of the principal symmetry axis of V_S , and its value will also depend on S . We then let

$$\begin{aligned} S_z'' &= S_z \cos(\theta - \varphi_S) + S_x \sin(\theta - \varphi_S), \\ S_z' &= S_z \cos \varphi_S - S_x \sin \varphi_S. \end{aligned} \quad (10)$$

Substituting these expressions into Eq. (6), and adjusting φ_S such that the term in $S_x S_z$ vanishes, we find that

$$\tan 2\varphi_S = \frac{\sin 2\theta}{\beta_S D_c / 3\alpha_S D_e + \cos 2\theta}, \quad (11a)$$

$$D_S = \frac{3}{2}\alpha_S D_e [3 \cos^2(\theta - \varphi_S) - 1] + \frac{1}{2}\beta_S D_c [3 \cos^2 \varphi_S - 1], \quad (11b)$$

$$E_S = \frac{3}{2}\alpha_S D_e \sin^2(\theta - \varphi_S) + \frac{1}{2}\beta_S D_c \sin^2 \varphi_S. \quad (11c)$$

Thus, according to this theory, we expect the observed zero-field splittings for each of the spin states, as well as the symmetry axes of the ESR spectra, to depend only on the two parameters D_e and D_c .

VIII. RESULTS AND DISCUSSION

In making the comparison between theory and experiment, we have taken the known pieces of experimental data and have obtained a best fit of these data to the theory. Table II shows the comparison. A principal result is that we can determine values for D_e and D_c . We find

$$\begin{aligned} D_e &= -0.058 \pm 0.005 \text{ cm}^{-1}, \\ D_c &= -0.191 \pm 0.005 \text{ cm}^{-1}. \end{aligned} \quad (12)$$

We note, in particular, that within our experimental uncertainty, the value of D_c is found to be equal to that for the isolated ions, for which $D_c = -0.191 \text{ cm}^{-1}$. From our experimentally determined value of D_e , and the known value of the dipolar interaction, we can determine a value for D_E , the anisotropic exchange interaction. We find, with $D_d = -0.037 \text{ cm}^{-1}$, that

$$D_E = D_e - D_d = -0.021 \pm 0.005 \text{ cm}^{-1}. \quad (13)$$

We note that the value found for D_E is quite small.

In general, we can say that the fine structure of the fourth-nearest-neighbor ground states is rather well described by our simple theory. It also appears from our value for D_c that the combined effect of the spin-orbit coupling and the crystal field, which gives rise to the ground-state splitting of the single ion, is not changed by the presence of a neighboring chromium ion. It is also apparent that such a term is primarily responsible for the observed ground-state fine structure of the fourth-nearest-neighbor pairs.

Our main emphasis in this paper has been on the nature of the ground-state energy levels of an exchange-coupled pair, for which the technique of detecting the spin resonances optically has proved invaluable. The main virtue of the technique is that it selects, from among the many resonances arising from a variety of different paramagnetic systems within the crystal, those resonances arising from a particular system, in this case, those associated with fourth-nearest-neighbor pairs. A second attractive feature of this technique is that it allows one to study paramagnetic resonances in optically excited states, and to study the details of exchange interactions in these states much as we have done here for the ground states. A third virtue of this technique is that it allows one to study some of the aspects of the energy transfer mechanisms giving rise to the fluorescences from dilute impurity traps, such as the fourth-nearest-neighbor fluorescence here.

ACKNOWLEDGMENTS

We should like to thank Professor Arthur Schawlow for his continued encouragement and helpful discussions throughout this work. We also should like to gratefully acknowledge the help of Susan Nichparenko and Garret Tollkuhn in the performing of many of the experiments.

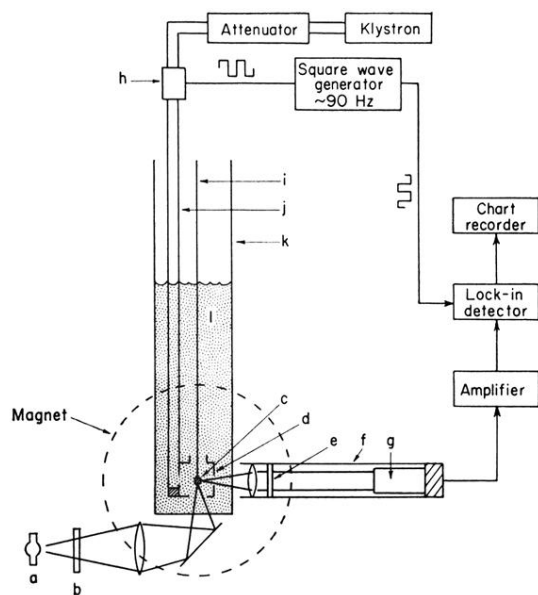


FIG. 2. Schematic diagram of apparatus for optical detection of spin resonances. a, 200-W mercury short-arc lamp; b, copper-sulfate filter; c, ruby sample; d, microwave cavity; e, 7009 Å narrow-band interference filter; f, light pipe; g, S-20 phototube; h, microwave modulator; i, shaft for rotating sample; j, waveguide; k, helium Dewar; l, liquid helium.